Available online at www.sciencedirect.com
SCIENCE DIRECT®
Surface Science 554 (2004) 90–102
SURFACE SCIENCE
www.elsevier.com/locate/susc

Modeling of the carbon-rich c(4×4) reconstruction on Si(1 0 0)

I.N. Remediakis [a,b], C. Guedj [a,b], P.C. Kelires [a,b,*], D. Grützmacher [c], E. Kaxiras [d]

[a] Department of Physics, University of Crete, P.O. Box 2208, 710 03 Heraclion, Crete, Greece
[b] Foundation for Research and Technology-Hellas (FORTH), P.O. Box 1527, 711 10 Heraclion, Crete, Greece
[c] Micro-and Nanostructures Laboratory, Paul Scherrer Institute, CH-5232 Villigen-PSI, Switzerland
[d] Department of Physics and Division of Engineering and Applied Sciences, Harvard University, Cambridge, MA 02138, USA

Received 29 October 2003; accepted for publication 13 February 2004

Abstract

The structure and energetics of the carbon-rich c(4×4) surface reconstruction on Si(0 0 1) is studied theoretically. These combined analyses demonstrate that for five or six carbon atoms per c(4×4) unit cell, the configuration involving carbon atoms in second nearest-neighbor positions in subsurface sites is more stable than the first nearest-neighbor configuration, involving a C–C dimer and a missing Si dimer. This SiC-like configuration could account for the formation of 3C–SiC precipitates generally observed during the growth of Si–C alloys for high C concentrations (>3%) and at high temperatures (>650 °C).

Keywords: Density functional calculations; Monte Carlo simulations; Scanning tunneling microscopy; Surface relaxation and reconstruction; Silicon carbide

1. Introduction

The structure of the carbon-induced c(4×4) reconstruction on the Si(1 0 0) surface has been the subject of intense investigations over the last years [1–10]. The change from the well-known c(2×4) or p(2×2) reconstructions of the pure Si surface to the c(4×4) pattern, with four dimers per unit cell, takes place after carbon (C) deposition at 600 °C. The debate concerning the structure of this pattern revolves around the following questions: (i) What is the profile of C atoms in the surface and subsurface layers? (ii) Do C atoms form C–C dimers on the surface or just Si–C dimers? (iii) Are there any defects, such as missing dimers involved in the picture? (iv) Do C atoms form particular complexes? (v) Do C atoms participate directly in the reconstruction?

Regarding the last issue, there have been reports [2,10] suggesting that the reconstruction is formed even at very low C contents, below 0.1 monolayer (ML) coverage, corresponding to less than one C atom per c(4×4) unit cell. This means that C does not need to be a regular part of the reconstruction, but that it can induce the c(4×4) pattern through the strain field produced by its incorporation. This

* Corresponding author. Address: Department of Physics, University of Crete, P.O. Box 2208, 710 03 Heraclion, Crete, Greece. Tel.: +30-2810-394223; fax: +30-2810-394201.
E-mail address: kelires@physics.uoc.gr (P.C. Kelires).

0039-6028/$ - see front matter © 2004 Elsevier B.V. All rights reserved.
doi:10.1016/j.susc.2004.02.016

is a viable scenario for such low contents, and we discuss it in detail below.

The possibility for the formation of C–C dimers, in general terms not specifically dealing with the c(4×4) reconstruction, was proposed by Kelires and Kaxiras [11] who performed ab initio calculations and Monte Carlo (MC) simulations of C incorporation in Si(1 0 0) using (2×1) cells with a high (1 ML) C coverage. A C–C dimer bond gives a large gain in chemical energy but also a large cost in strain energy due to the large deformations accompanying this structure. In the static calculations of Ref. [11], the C–C dimer bond was found to be the lowest-energy configuration among others involving a pair of C atoms in the near surface region. The gain in chemical energy partly overwhelms the strain-energy cost. The MC finite-temperature simulations, however, showed that C atoms readily diffuse at typical growth temperatures from the fully covered with C–C dimers surface into sub-surface sites, in agreement with experimental work by Osten et al. [12]. An oscillatory composition profile is produced characterized by enhancement of C concentration in layers 1 and 3, a near depletion in layer 2, and reduction in layer 4. The most probable subsurface positions of C atoms are in third nearest-neighbor (NN) distances, as in the bulk configurations in $Si_{1-x}C_x$ alloy layers suggested by Rücker et al. [13].

Therefore, the finite-temperature MC simulations in the work of Ref. [11] gave clear evidence for subsurface C. In fact, when the surface was initially prepared to consist of Si–C dimers, the simulations showed a further enhancement of subsurface C. Subsequent work by Remediakis et al. [9] focusing exclusively on the c(4×4) reconstruction confirmed the existence of both surface and subsurface C. However, the static calculations in the work of Ref. [11] neglected to examine the possibility to have a C atom on the surface forming a Si–C dimer bond and another C in subsurface positions. This negligence was corrected in the work of Ref. [14]. It was found that the configuration involving a Si–C dimer in a (2×1), or (2×2), unit cell and another C atom in sites of layer 3 (or 4) below the surface dimers, which are under compressive stress and thus favorable for the smaller atom (C) [15,16], is lower in energy than a C–C dimer bond by $\simeq$0.1 eV/(C pair). Subsequent work [7,8] confirmed this picture reached by Kelires [14].

Among the models proposed for the c(4×4) reconstruction of the C-rich surface, three recent models explored the possibility to have both surface and subsurface C. The first of these models, proposed by Leifeld et al. [5], requires the formation of carbon clusters of six first NN C atoms, consisting of C–C dimers bonded to four C atoms in the second subsurface layer. This configuration was found to explain the apparent pairing of Si dimers seen in STM images, in the presence of strain-relieving missing dimers, but it does not account for the presence of C in the third or forth subsurface layers, as is indicated by XPS [3,17] and XPD [17] experiments. The models of Remediakis et al. [9] and Simon et al. [8] take this into account. The former is based on the theoretical C composition profile in Refs. [11,14]. It considers C atoms on the surface forming Si–C dimers and in the third layer at the favorable compressive sites. The latter model also considers as basic surface ingredient the Si–C dimers, it is even more flexible by in addition allowing occupancies in the forth layer, and seems to be compatible with XPS and STM measurements. Common characteristic of both models is the absence of C at the second subsurface layer, and the correlation of C atoms at third NN positions. Such c(4×4) configurations can be considered as precursors for the growth of $Si_{1-x}C_x$ alloys.

In this paper, we offer an alternative model for the C-rich c(4×4) reconstruction. The configuration contains five C atoms positioned at second NN arrangements, forming a cubic β-SiC cluster below the surface. We use ab initio density functional theory calculations to obtain the relative energies and simulated STM images of the considered structures and Monte Carlo simulations to study their stability and thermodynamical properties. We find that the energy of the new configuration is lower than the Leifeld structure, and its computed STM image compares favorably with new experimental STM images. We propose that this new c(4×4) configuration could be considered as a precursor for the growth of ordered β-SiC alloys.

2. The configurations

All configurations studied in this work have the c(4×4) periodicity. The configurations are named *NX*, *N* being the number of C atoms in the c(4×4) unit cell and *X* an index to distinguish structures of the same *N*. In particular, configurations indexed as *A* (5*A* and 6*A*) are obtained by substituting the appropriate Si atoms by C in pure Si(1 0 0) (configuration 0*A*). Configurations indexed as *B* (5*B* and 6*B*) are obtained by substituting the appropriate Si atoms by C in Si(1 0 0) with a missing dimer defect (configuration 0*B*). The relaxed geometries of the considered configurations are shown in Fig. 1.

Configuration 0*A* is the pure, dimer reconstructed Si(1 0 0) in the c(4×4) periodicity. The dimers are shown in Fig. 2 as pairs of large gray spheres. The two atoms forming the dimer do not lie in the same height, i.e, the dimer is tilted. Adjacent dimers are tilted in opposite directions, forming a local p(2×2) arrangement. 0*B* corresponds to pure Si(1 0 0) with an isolated missing dimer defect. The distance between subsequent missing dimers is 15.4 Å, large enough to ensure negligible coupling between defects.

The configurations with six C atoms per c(4×4) cell (6*A* and 6*B*) contain C atoms at first NN positions and a C–C dimer on the surface. The atoms are in positions 1, 2, 3, 4, 5 and 6 of Fig. 2. The configuration including a missing dimer, 6*B*, was proposed by Leifeld et al. [5] as a good candidate to account for the observed STM images. As discussed above, C atoms are not expected to be in nearest-neighbor positions in bulk $Si_{1-x}C_x$ alloys [11,13], and C–C dimers are quite rare in annealed C–Si(1 0 0) samples [4]. However, C–C dimers could exist in the presence of strain-relieving missing dimers. We study here this configuration together with a similar one but with no dimer missing (6*A*).

We consider two new structures for C-alloyed Si(1 0 0), with five C atoms per unit cell. They are configurations 5*A* and 5*B*, with C atoms in positions 3, 4, 5, 6 and 7 of Fig. 2. These structures contain C atoms in second NN positions, which form a β-SiC cluster below the surface. Formation of SiC clusters during C incorporation on Si(1 0 0) has been previously reported [12]. In addition, the structures have a C atom at the fourth layer directly below the surface dimer. This site is under compressive stress due to the reconstruction [15,16] and is expected to be favorable for C.

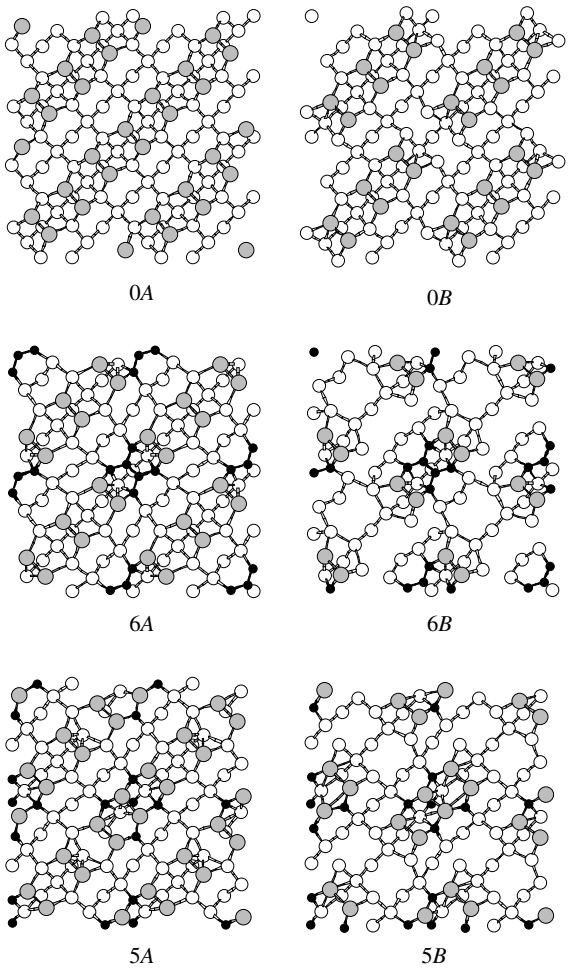

Fig. 1. Relaxed geometries (top views, topmost four layers shown) of the configurations discussed in the text. A supercell four times the c(4×4) unit cell is shown. The configurations on the right column, marked *B* contain a dimer vacancy defect. Si surface atoms are shown as grey spheres, Si atoms of the 2nd, 3rd and 4th layers are shown as smaller, white spheres; C atoms are represented by black spheres.

3. Method

The need for combining different theoretical methods in this study arises from the nature of the

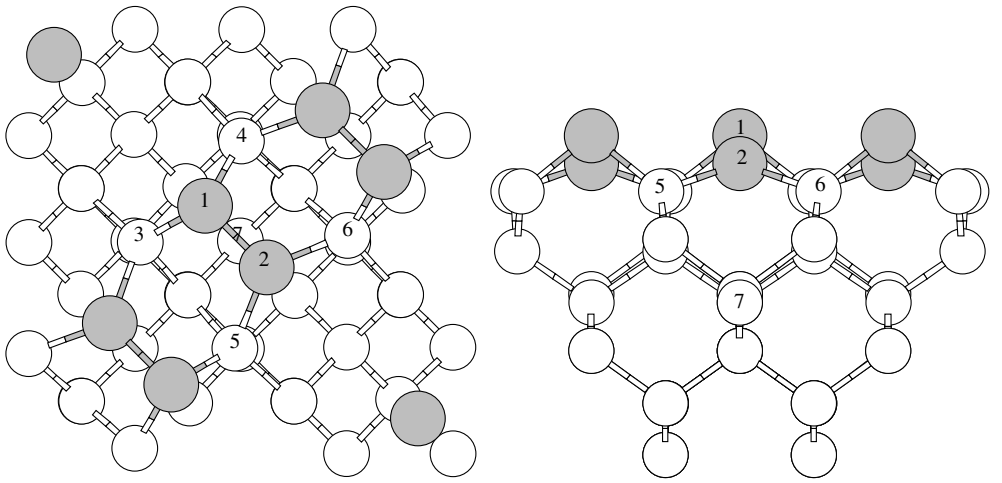

Fig. 2. Top (left) and side (right) views of a c(4×4) unit cell of the dimer-reconstructed Si(1 0 0). Dimer atoms are shown in gray. The numbers denote sites where C substitutes Si atoms in the configurations discussed in the text.

properties of interest. In the microscopic level, the large differences in covalent radii (35%), bond enthalpies (35%) and electronegativities (25%) between C and Si, suggest that the strongly distorted bonds and the charge-transfer effects present in the system establish the necessity for quantum mechanical calculation of the total energies and forces.

On the other hand, the calculation of the free energy in a quantum mechanical scheme for large-size systems, as the ones under study here, is either unfeasible or approximate. For this purpose we employ Monte Carlo calculations using empirical potentials. This approach allows us not only to calculate the free energy of the system at any temperature, essentially at the accuracy of the empirical potential we chose, but also to explore diffusion of atoms, transformations of the system and possibly phase transitions between different configurations.

3.1. Ab initio method

We model the system by a repeated slab geometry, having seven layers of Si atoms and a terminating H layer at the bottom. The Si layer above the H atoms is kept fixed during the simulation, with the positions of H chosen in such a way to mimic the bulk Si–Si bonds. The other six Si layers are allowed to move. The system has the c(4×4) periodicity with the lattice constant taken to be that of bulk Si. The repeated slabs are separated by ≈10 Å of vacuum. This choice of supercell has been proven excellent for the description of both pure and C-enriched Si(1 0 0) [9].

The first-principle calculations were performed using the commercial Vienna ab initio simulation package (VASP) code [18–20], based on density functional theory (DFT) [21,22]. The exchange and correlation energy and potential were calculated using the generalized gradient approximation (GGA) functional of Perdew and Wang [23]. The atomic cores and their interactions with valence electrons were taken into account via the ultra soft Vanderbilt type pseudopotentials [24] as supplied by Kresse and Hafner [25].

The Brillouin zone of the system was sampled by the Γ point, which is sufficient due to the large size of the unit cell. Indeed, convergence tests by Sonnet et al. in Ref. [7] showed that increasing the k-points used for a C-rich c(4×4) Si(1 0 0) unit cell does not result in significant changes in the energetics. The wave function was expanded to plane-waves using a cut-off energy of 26 Ry. For fixed ionic positions, the wave functions are calculated using a preconditioned conjugate gradient minimization algorithm, until the total energy is

converged up to 10^{-4} eV. In each self-consistency step, the output charge density is mixed with the input one using a Pulay mixing method [26]. The ionic positions are relaxed using a conjugate gradient minimization algorithm, until the difference in the converged total energies before and after each ionic step is smaller than 10^{-3} eV.

The STM images were obtained from the calculated wave functions by means of the Tersoff and Hamann theory [27]. In this scheme the tunneling current is proportional to the local density of states at the microscope tip, integrated in a window of energies from $-V$ to E_F, where V is the voltage between tip and surface, and E_F is the Fermi level of the system. We can thus calculate the tunneling current I as a function of the surface coordinates (x, y) and the tip–surface distance z. To simulate the constant-current mode of the STM, we solve numerically the equation $I(x, y, z) = I_0$ with respect to z, and then draw a contour plot of z as a function of x and y.

It is well known that although the dimers of Si(1 0 0) are tilted, with one atom located higher than the other, they appear symmetric at STM images taken at room temperature. The reason is that due to thermal vibrations of atoms, dimers flip at a frequency much higher than what the STM tip can capture [28]. The room temperature STM image is thus an average over the two possible configurations of each dimer. Alternative explanations of this effect involve the tip–dimer interaction, which favors the dimers in a particular tilted direction, and which reverses when the tip is over the other end of the dimer. To make our simulations directly comparable to the observation, we also symmetrize the derived STM images: for each (x, y) point of the surface, we plot the average of the tip height at this point and at the symmetric point with respect to the dimer row.

3.2. Monte Carlo method

We perform continuous-space Monte Carlo (MC) simulations. The energy of the system is obtained using the multi-component empirical potentials of Tersoff [29], applied with success in similar contexts [11,14,30]. Equilibration of the system is done at 900 K [14,30,31]. For positional equilibration, there are two types of MC moves involved in the algorithm: the random atomic displacements and the volume changes. A third kind of move leads to configurational equilibration, which is needed to check the stability of the structures at a given temperature against either randomization or transformation to another phase. This kind of moves consists of Ising-type identity flips, restricted to the form of mutual particle interchanges, e.g., from C to Si at a randomly chosen site and vice versa at another site, keeping the composition constant. To overcome the large barriers associated with C incorporation and exchange, Kelires [30] has introduced a relaxation of the nearest neighbors of the atoms that exchange identities before the energy is recalculated. The resulting statistical ensemble can be described as the familiar isobaric-isothermal (N, P, T) ensemble supplemented by the identity switches.

The traditional random atomic moves $s^N \to s'^N$, s^N is symbolic for the $3N$ scaled atomic coordinates in the cell, and the volume changes $V \to V'$ are accepted with probability

$$P_{\text{acc}} = \text{Min}[1, \exp(-\Delta W/k_B T)], \tag{1}$$

where

$$\Delta W = \Delta U_{\text{displ}}(s^N \to s'^N) + P(V' - V) - Nk_B T \ln(V'/V). \tag{2}$$

For the identity flips the acceptance probability is given by

$$P_{\text{acc}}^{\text{iden}}(i \leftrightarrow i') = \text{Min}[1, \exp(-\Delta U(s^N)/k_B T)], \tag{3}$$

where $\Delta U(s^N)$ denotes the change in the potential energy due to the identity $(i \leftrightarrow i')$ mutual flip and the accompanying relaxations [30]. The implementation of this ensemble is done according to the Metropolis algorithm [32].

For the MC simulations we model the system by a supercell consisting of four c(4×4) cells with seven layers of Si atoms. The bottom layer is fixed to the bulk positions. The lattice vectors parallel to (1 0 0) are kept fixed to their values for bulk Si, and the lattice vector perpendicular to (1 0 0) is relaxed, allowing the layer separation distance to change in order to minimize the total energy.

3.3. Comparison of energies

To compare the energies of the structures, we must take into account the fact that they contain different number of atoms, and so we need to use the grand canonical ensemble formalism. For this purpose we calculate the grand thermodynamical potential,

$$\Omega(NX) = F_{\mathrm{tot}}(NX) - N\mu_{\mathrm{C}} - N_{\mathrm{Si}}\mu_{\mathrm{Si}}, \quad (4)$$

where $F_{\mathrm{tot}}(NX)$ is the calculated total free energy of configuration NX, N and N_{Si} is the number of C and Si atoms in configuration NX. μ_{C} and μ_{Si} are the appropriate chemical potentials for C and Si, respectively. The chemical potentials tune the stoichiometry of the system and are extremely important in the prediction of the favorable structure [33,34].

We define the relative energies of the cells with respect to $0A$, the pure Si(1 0 0),

$$E_{\mathrm{r}}(NX) = \Omega(NX) - \Omega(0A) \quad (5)$$

and the formation energy, which is the energy difference between NX and $0X$:

$$E_{\mathrm{f}}(NX) = \Omega(NX) - \Omega(0X). \quad (6)$$

The relative energy, $E_{\mathrm{r}}(NX)$, is the amount of energy needed to remove N Si atoms from pure Si(1 0 0) (configuration $0A$), put them in bulk Si, and substitute them with C atoms taken from the appropriate reservoir. For the structures labeled B, which contain a missing dimer, $E_{\mathrm{r}}(NX)$ includes the energy cost to remove the dimer. In contrast, the formation energy, $E_{\mathrm{f}}(NX)$, is the amount of energy required to remove N Si atoms from either pure Si(1 0 0) or Si(1 0 0) with a missing dimer (configuration $0X$), put them in bulk Si and substitute them with C atoms. In other words, those two energies correspond to the enthalpies of the reactions:

$$(0A) + NC \rightarrow (NX) + (N + 2\delta_{XB})Si - E_{\mathrm{r}}(NX) \quad (7)$$

and

$$(0X) + NC \rightarrow (NX) + NSi - E_{\mathrm{f}}(NX). \quad (8)$$

The term δ_{XB} is 1 when configuration is labeled B and contains a missing dimer. In those reactions, Si is always in bulk phase, since Si bulk is the natural reservoir for Si atoms. Atoms can always be added to, or taken from bulk Si by means of step evolution. On the other hand, an a priori choice for the phase of C (and hence μ_{C}) is not possible without reference to a particular experiment. For this reason, we calculate the energies of the structures as *a function* of μ_{C} in the range from 0 (energy of a C atom) to −7.37 eV, the chemical potential per atom of diamond. *This is the lower bound in the possible values of the carbon chemical potential, and cannot be exceeded.*

4. Results and discussion

4.1. Structural properties and energetics

The relaxed geometries for all six configurations described in Section 2 are shown in Fig. 1. Their relative and formation energies are given in Table 1, where μ_{C} is taken as the energy of a C atom in diamond. The second row of Table 1 shows the position of C in the c(4×4) unit cell, according to the numbering scheme of Fig. 2. We first compare the energies of configurations with the same C content; we then compare cells of different C content, discussing the dependence of the energies on C chemical potential.

In configuration $0B$, the missing dimer is in the center of the frame. The second layer dimer atoms below the dimer form elongated bonds (not drawn in Fig. 1) of length 2.73 Å, 16% longer than the bulk bond length of Si (2.35 Å), in agreement with the calculated length of 2.79 Å by Wang et al. [35]. The calculated formation energy of the defect, 0.25 eV per missing dimer, is in excellent agreement with calculated values of 0.22 eV [35] and 0.28 eV [36]. The dimers adjacent to the defect have lengths of 2.33 Å, and are slightly longer than the other dimer of the unit cell (2.26 Å). For comparison, the calculated dimer bond length for configuration $0A$ is 2.34 Å. The bonds between the dimer atoms and the second layer atoms are elongated to 2.45 Å on average; they are 2.35 Å on average in $0A$. The dimers next to the defect are parallel to the surface, eliminating the characteristic buckling of the (2×1) reconstruction. The bond angles are also restored close to the tetrahedral value in the missing dimer

Table 1
Relative and formation energies for the various configurations considered according to Eqs. (5) and (6) in eV per c(4×4) cell

Configuration	0*A*	0*B*	6*A*	6*B*	5*A*	5*B*
C atoms	–	–	[1,2,3,4,5,6]		[3,4,5,6,7]	
$E_r(NX)$	0.00	0.25	7.94	6.99	3.16	3.75
$E_f(NX)$	0.00	0.00	7.94	6.74	3.16	3.51
$E_r^{(2)}(NX)$	0.00	1.39	10.1	8.84	4.02	4.12
$E_f^{(2)}(NX)$	0.00	0.00	10.1	7.45	4.02	2.73

$E_r^{(2)}$ is the free energy difference at 900 K, calculated with the Monte Carlo method. μ_C is taken as the energy of a C atom in diamond. The numbers in the second line after each configuration name indicate the position of C atoms, according to the numbering scheme of Fig. 2.

configuration. There are two competing effects in this configuration: the reduction of dangling bonds from 8 (in 0*A*) to 6 per unit cell and the restoration of bond angles, which lowers the total energy, and the distortion of bond lengths, which raises the total energy. This competition results in the calculated very low energy difference between 0*A* and 0*B*.

Configuration 6*A* contains six C atoms at first NN positions. Two of them form a C–C dimer of length 1.51 Å, slightly shorter than the bulk bond length in diamond of 1.54 Å. The other four C atoms are each connected to a C atom of the dimer (bond length 1.58 Å), a Si atom of a Si–Si dimer (bond length 2.01 Å), and two Si atoms of the third layer (bond lengths 2.06/1.97 Å). All C–Si bonds are longer compared to the Si–C bond in β-SiC, which is 1.89 Å. The Si–Si dimers neighboring the C–C dimer have same length as the dimers on pure Si(1 0 0) (0*A*). The other Si–Si dimer is elongated, its length being 2.37 Å. All three dimers of configuration 6*A* are flat.

In 6*B*, which is the same as 6*A* with a missing dimer, the C–C dimer is shorter (1.45 Å); at the same time, the angles formed by the C atoms of the dimer are very close to 120°, indicating that the C atoms are both in an sp^2 hybridized state. The bond lengths of a second-layer C atom with a C atom of the C–C dimer are 1.55 Å long, almost unstretched. The C–Si bonds are also closer to the SiC bond length compared to configuration 6*A*. Because stretching or bending of the C–C bonds costs more energy than destorting Si–C or Si–Si bonds, the system gives priority to the satisfaction of the C bonds. This results in the twisted dimers shown in Fig. 1; the dimers are tilted and have length very close to the dimer length in pure Si(1 0 0). The missing dimer allows for this relaxation to take place, relieving in this way the strain introduced by the large C content of the unit cell. This is the reason for the lower energy of configuration 6*B* compared to 6*A*.

Configuration 5*A* contains five C atoms at second NN positions, forming a small SiC cluster below a Si–Si dimer. The symmetry of the c(4×4) reconstructed Si(1 0 0) has broken, and the dimer above the SiC cluster moves to the left, as shown in the relative panel of Fig. 1. As a result, the four dimers of the unit cell have all different lengths. The dimer above the C atoms is tilted and elongated (2.41 Å); the same applies to the dimer that has come close to it (length 2.40 Å). The other dimer connected to C atoms is shorter (2.32 Å), while the fourth dimer, which is not connected to C atoms is flat and 2.38 Å long.

The C atoms lying between the two dimers that have come close to each other form bonds of lengths between 1.82 and 2.00 Å, with angles between 115° and 122°; apparently, they are in a close sp^2 hybridized state with the surrounding Si atoms. The arrangement of C atoms is thus qualitatively different from that of bulk SiC, where π bonding is absent. The other C atom in the forth layer forms four bonds of lengths 1.88, 1.94, 1.94 and 1.99 Å, as close to the bond length in bulk SiC as the system can allow.

In configuration 5*B*, obtained from 5*A* by removing a dimer, we observe the same symmetry breaking as in 5*A*. The dimer above the C atoms has moved from its symmetrical position, and is again elongated (2.40 Å). The dimer close to it is 2.36 Å long, while the other one is 2.50 Å long.

Again, the C atoms in the second layer are close to an sp^2 configuration, but this time the angles have a more broad dispersion from 120°, indicating an intermediate hybridization of C. The other C atom in the forth layer forms bonds of almost identical lengths and angles as in 5*A*. The distance between two Si atoms of the second layer at the dimer vacancy site is 4.83 Å, meaning that no bond has formed.

In contrast to the case with six C atoms per unit cell, for five C atoms the presence of the missing dimer does not lower the energy of the system. Configuration 5*B* has lower relative energy than 5*A* by 0.59 eV per unit cell. The difference in formation energies is smaller, 0.35 eV per unit cell.

In Fig. 3 we plot the relative energies of the considered structures as a function of the C chemical potential, or equivalently, the free energy per C atom of the C reservoir. We observe three changes in the preferred configuration: For low μ_C, where C is strongly bound, 0*A* is the lowest energy structure. For this region of μ_C it is costly energetically to remove C from the reservoir and add it to the system. The first transition happens for $\mu_C \approx -6.8$ eV. From this point, configuration 5*A* is the energetically favorable one, up to $\mu_C \approx -3.6$ eV where configuration 6*B* becomes the one having the lowest energy. As we move to lower values of the chemical potential, it becomes easier to remove

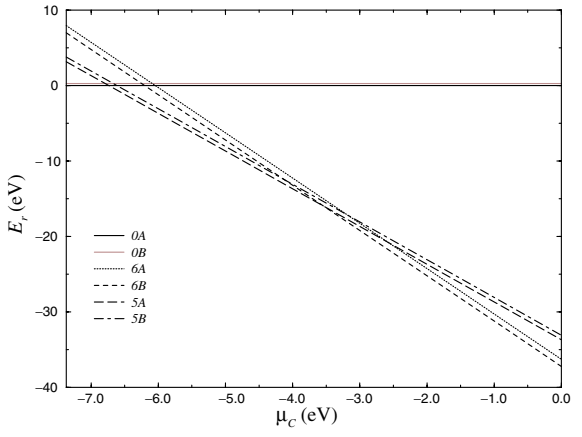

Fig. 3. Relative energies of the considered structures, according to Eq. (5), as a function of the C chemical potential, as derived from the ab initio calculations at zero temperature. Energies are given in eV per c(4×4) unit cell.

C atoms from the reservoir, and because C forms stronger bonds than Si, structures with larger C content are favored.

The chemical potential of C is the free energy per atom, relative to a free C atom, in the C reservoir with which the system is in thermal equilibrium. It can be either a solid, which is represented here by diamond, a typical form of solid C, or it can be a gas of C clusters. The latter is most likely the case in chemical vapor deposition (CVD) experiments. Carbon clusters C_n with $4 \leqslant n \leqslant 32$ have chemical potentials in the range between −7.1 and −5.2 eV per atom [37], while all structures with $n < 20$ have chemical potentials above −6 eV per atom. So in conditions of ordinary CVD experiments, the configuration 5*A* will be favored. In molecular beam epitaxy (MBE) growth, the C beam can in principle consist of single atoms or very small clusters consisting of two or three C atoms; in such cases the situation will be more complex. For two or three C atoms in the clusters, either configuration 5*A* will still be favored, or 5*A* and 6*B* will coexist. For monomers, 6*B* is expected to dominate. Note, however, that this is the zero-temperature picture and not the one corresponding to the actual growth conditions.

In our earlier work in Ref. [9], we considered structures involving four, or less, C atoms in the c(4×4) unit cells. All these structures are relevant to values of the chemical potential lower than ∼−6.5 eV, at which point the transition from the structure with 4 C atoms to 5*A* takes place. Thus, for higher values, 5*A* and then 6*B* are favored.

In order to determine the thermodynamics of the system and extract the relative energies at the typical growth conditions, we performed finite-temperature MC simulations at 900 K by the method described earlier. No identity switches are performed at this stage. The calculated free energy differences are given in Table 1. (The zero-temperature values are all a bit lower by ∼0.3–0.5 eV.) We find exactly the same ordering for the relative energies as in the ab initio calculations. However, the two transition points discussed before are in the MC calculations shifted to approximately −6.5 eV for the transition from 0*A* to 5*A* and −2.5 eV for the transition from 5*A* to 6*B*. Thus, in the picture more relevant to the experiment, configuration 5*A* will be

the favored structure over most of the range of C chemical potential and deposition conditions, but still configuration 6*B* has considerable chances to dominate or coexist with 5*A*.

By switching on the identity flips in the algorithm, we checked the stability of configuration 5*A*. A similar check has been earlier done for the 6*B* structure in the work of Ref. [5]. We find that at 900 K, the structure is very stable against interchanges of C and Si atoms. As with the 6*B* configuration, there is a slight tendency for switches at higher *T*'s, but for a significant rate, that would randomize the structure, temperatures higher than 1500 K are needed. We conclude that if the structure can be formed at usual growth conditions, then it will be stable.

These results bear significance for the problem of growth of highly concentrated C-alloy layers in Si. It is usually assumed that such layers cease to be accessible to diffusion as further material is deposited on top, and so they become buried and the relevant geometries are frozen in. Assuming that this freezing-in mechanism governs the growth of thicker layers, we can conclude that the models described earlier [8,9,11] could be thought of as precursors for the growth of $Si_{1-x}C_x$ alloys, having C atoms arranged in third NN positions. The interesting thing is that the present model of configuration 5*A* can be considered as a precursor for the growth of ordered β-SiC alloys. We are not saying that thick SiC layers can be grown at this low temperature (600 °C). We are rather saying that SiC-cluster configurations already exist as local structures in the c(4×4) reconstruction pattern, even at this temperature, and that they are able to coalesce by annealing at higher *T*'s (>650 °C). This is energetically much less costly than rearranging Si_nC aggregates.

Osten et al. [12] measured C 1s core-level binding energies in C-rich (1 ML) surface layers in Si and found two prominent peaks. One near 282.8 eV at 650 °C, which they attributed solely to Si_4C structures, and one at 282.6 eV by annealing at 920 °C, typical for SiC alloy on Si. Considering the proximity of the two peaks, it is tempting to suggest that the former is not due to Si_4C structures alone, but it could contain a component due to SiC microclusters. This proposition is strengthened by considering that the β-SiC subsurface clusters are distorted, as we discussed above, containing a certain degree of π bonding, and this might be able to slightly shift the binding energies to the direction of graphitic values.

The two things that differentiate the β-SiC cluster model from the Si_nC models are the second NN correlation of C atoms, and the presence of C atoms in the second subsurface layer. The former does not contradict previous conclusions regarding the relative positioning of C atoms in the bulk Si lattice [13,30], because either these conclusions were based on static calculations in the dilute limit, which considered correlations of only *pairs* of C atoms [13], or on dynamical simulations [30]. For more C atoms approaching to form a cluster, the lowest-energy local configuration is definitely a SiC microcluster, but the energy barrier to percolate these clusters to form a SiC alloy is high, and thermal activation is needed. The barrier for simulations to reach dynamically this configuration is also high. The C occupation of sites in the second subsurface layer, on the other hand, is not unexpected if we recall that these sites are all under large compressive stress due to the reconstruction [15], and so favorable for C, provided that the C population in the surface layer and in the third layer is minimal to avoid the repulsive first NN interaction of C atoms. Thus, for the C-rich surface we are talking about, the β-SiC cluster model for the c(4×4) reconstruction is a quite probable scenario, and the following discussion based on STM images confirms it.

4.2. Simulated STM images

To make our simulations readily comparable to experiment, we performed simulations of the STM images arising from each of the configurations studied here, using the Tersoff–Hamann theory as described in Section 3.1. The simulated STM images are shown in Fig. 4. They are all taken at a bias voltage of −2.5 eV, probing thus the occupied states of the system.

The pure Si(1 0 0) configuratons, 0*A* and 0*B* show the characteristic bean-shaped white dots above each dimer. In configuration 0*B*, no signal is obtained above the missing dimer, because the

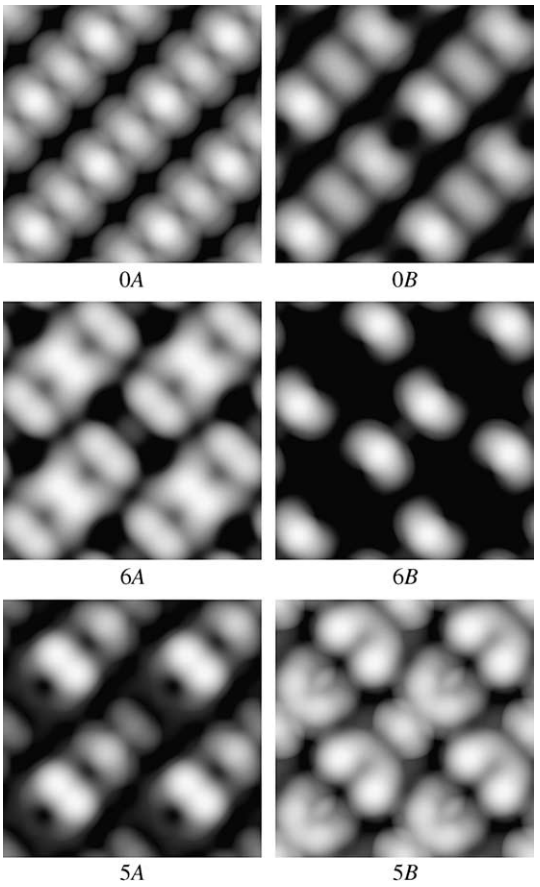

Fig. 4. Simulated STM images for all configurations of Fig. 1. Constant-current mode at a bias voltage of −2.5 V, occupied states probed.

topmost atoms in this region are much lower than the dimer atoms, and the tunneling current decreases exponentially with increasing tip–surface distance. This is the reason why some dimers appear brighter than the others, as their center lies higher by approximately 0.1 Å.

The simulated STM image for configuration 6*A* looks very similar to that for 0*B*. The black region inside the dimer row corresponds to the C dimer, which is invisible in STM, due to the lower geometrical position and the lower energy of the bonding states of the C–C dimer compared to the Si–Si dimers [5,38]. The two Si–Si dimers neighboring the C–C dimer are lower than the other one, which appears as a brighter spot. In configuration 6*B* this dimer is missing, so the only atoms appearing in the STM image are those belonging to the two Si–Si dimers. This image is essentially the same as that simulated by Leifeld et al. [5].

Configuration 5*A* gives an STM image characterized by two large bright spots and a smaller one. Two large bright spots characterize also the STM image corresponding to configuration 6*B*; the contrasting difference is the obvious assymmetry between the brightness of the two spots. The large bright spot corresponds to the dimer that is not bonded to any C atom (see Fig. 1). The other white spot corresponds to the dimer that is bonded to two C atoms. The weak grey spot corresponds to the dimer bonded to four C atoms and lies above the SiC cluster. The fourth dimer of the unit cell, which is brought close to the one above the SiC cluster, does not give any measurable signal.

The simulated STM image for configuration 5*B* is qualitatively different from the others. The two large double spots correspond to second layer atoms, which would be bonded to a dimer, if there was no vacancy. Due to the presence of the vacancy and the strain introduced by C, those atoms have come higher than the dimers (see Fig. 1). The other spot between them corresponds to the Si dimer bonded to four C atoms; the other two Si dimers of the unit cell are invisible. There is an asymmetry in the four second layer atoms around the vacancy, as two of them are higher than the other two, so one pair of bright spots appears brighter than the other.

An experimental image of the C-alloyed Si(1 0 0) is shown in Fig. 5. The image is taken by the group of Grützmacher and is similar to that published by Leifeld et al. [5]. The amount of C deposited was 0.11 ML, and the reconstruction is not homogeneous, i.e., the c(4×4) regions do not cover the whole surface, but (2×1) patches are also observed. However, much of the C deposited is found in the c(4×4) areas. [1] The experimental STM image

[1] A strong evidence that C is mainly located in the c(4×4), and not in the (2×1), areas is provided by the observation that Ge islands, after Ge deposition on C-predeposited Si(1 0 0), are formed only on the (2×1) regions. See Ref. [39]. This is explained on the basis of the repulsive Ge–C interaction in the Si lattice. See Ref. [30].

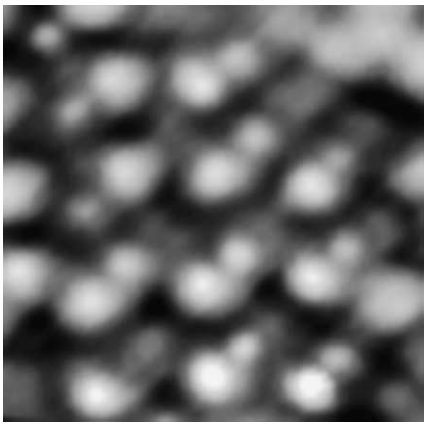

Fig. 5. High-resolution experimental STM image from C-alloyed Si(1 0 0).

refers to such an area. The bias voltage is −2 V and the current is 0.2 nA. The image contains characteristic pairs of spots arranged in a c(4×4) pattern. Both simulated STM images for 6*B* and 5*A* match this feature. However, the simulated image for 5*A* has the clear advantage of capturing the assymmetry between the brightness of the two spots. The elongated structure shown in the middle of the picture could be attributed to a 5*B* cell. Let us emphasize that, in accord with experiment, we propose our model configurations to cover only a part of the whole surface. Thus, when we speak about C-rich c(4×4) reconstruction, we do not mean a uniform coverage of the whole surface with configurations 5*A* (mainly) and 6*B*, but only coverage of the C-containing areas. Note also that the configuration 5*A*, although C-rich, does not produce excessive strain which could lead to disorder in the c(4×4) region, because it is β-SiC-like. In 6*B*, the missing dimers relieve part of the stress.

In another STM experiment published bu Maeng and Kim [40], the observed STM images show both characteristics of our simulated STM images for 6*A* and 6*B*; those structures are proposed as those producing the observed image. The relatively high energy difference between the two configurations renders their coexistence questionable. A co-existence of 5*A* and 6*B* would be more consistent with our results.

To make the comparison with experiment more quantitative, we calculated the distances between the pairs of spots in the simulated images. To do this, we first plot a cross-section of the simulated STM image. Fig. 6 shows cross-sections of the simulated STM images along the dimer row, averaged over a width of ±1.9 Å around the dimer line. We define the intrapair distance as the distance between the two highest maxima in the unit cell, and the interpair distance as the distance between the second peak and the next one, which belongs to the adjacent unit cell. The experimental values for intrapair and interpair distances are 5.9 and 9.6 Å, respectively.

For 0*A*, these distances are both 7.72 Å, the distance of two second-nearest neighboring dimers, which equals the lattice separation of the p(2×2) unit cell. In 0*B* the missing dimer has brought the remaining dimers closer, and the intrapair (interpair) distance is 6.9(8.5) Å, respectively.

For 6*A* the calculation is meaningless, as the two less bright spots surrounding the brighter one correspond exactly to the same height. For 6*B*, we find an intrapair distance of 5.6 Å and interpair distance of 9.8 Å, values that agree very well with experiment. For 5*A* we find an intrapair distance of

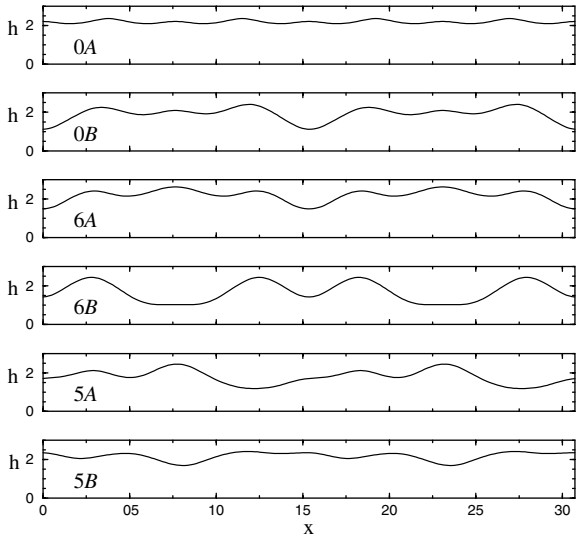

Fig. 6. Average profiles of the simulated STM images of Fig. 4 along the dimer row. *x* is the distance (in Å) from the lower left corner of each image in Fig. 4, and *h* is the height (in Å) from the topmost atom of the surface.

4.8 Å, and an interpair distance of 10.6 Å. In this case the two spots are closer compared to 6*B*. Finally, for 5*B* we find a larger separation of spots by 6.9 Å and a smaller interpair distance of 8.5 Å.

The calculated intrapair distance for the configurations with five C atoms per unit cell is smaller than the experimental by 1.1 Å for 5*A* and larger than the experimental by 1.0 Å for 5*B*. Because those two configurations were found to have formation energies differing by only 0.35 eV per unit cell, coexistence of the two could account for the observed length, since they produce STM images that match better the experimental image than configuration 6*B*, which agrees exactly with the observed distances between spots, but does not reproduce the assymmetry in their brightness.

As we mentioned in Section 1, an alternative picture for the c(4×4) reconstruction is given by the experimental work of Jemander et al. [10]. These authors proposed that with a deposition of only 0.07 ML of C they were able to get a homogeneous coverage of the whole surface with the c(4×4) reconstruction. Since the C content was low, it was concluded that C need not be a regular part in the reconstruction, i.e., C is not necessarily found in the c(4×4) unit cells, but that C induces the reconstruction through the strain field it generates when it is incorporated in the Si lattice. In our previous work in Ref. [9], where we treated the whole surface as uniformly covered with c(4×4) units, we also proposed structures without and with C alternating each other. Although the C-free configurations differ from Jemander's structures, which involve Si ad-dimers, they also indicate a partly strain-induced reconstruction. Thus, this alternative picture is quite possible. However, it should be emphasized that the present work does not refer to such a uniform coverage of the whole surface but, as we discussed above, to a non-uniform coverage of a part of the surface, as seen experimentally by Grützmacher's group. Therefore, our model does not contradict the model proposed by Jemander et al. Both are viable models, provided that both experimental observations (uniformity and non-uniformity of the reconstruction) are correct. Our theoretical work cannot shed light onto this. It seems that the uniformity or not of the reconstruction depends on the experimental conditions of growth and treatment of the surface, and needs certainly further discussion and experimental investigation. A general picture could be one where we have fluctuation of the C content per unit cell, such as the coexistence of 5*A* and 6*B*, along with regions without C or with four or less C atoms per unit cell.

5. Conclusions

It has been observed experimentally that when C is incorporated into Si(1 0 0) a non-uniform pattern arises with c(4×4) units covering part of the surface. These regions are C rich. In this case, structures involving C atoms at first- or second-nearest neighbor positions are necessary to be considered in order to explain the observed STM images. We propose four such configurations here, two of which contain a missing dimer. The energetics at temperatures relevant to the experiment show that the β-SiC cluster configuration 5*A*, characterized by arrangement of C atoms at second NN distances, is the favored structure over most of the range of C chemical potential and deposition conditions. Still, the configuration 6*B* involving a C–C dimer and a missing Si dimer has significant chances to dominate or coexist with 5*A*. The simulated STM images for both configurations look reasonably similar to the observation, but the image for the 5*A* structure has the advantage of capturing the assymmetry in the brightness of the spots. For less C in the unit cell, other models, such as the one by Simon et al. [8] would rather be favored. An alternative experimental picture is one with a uniform and complete coverage of the surface with the c(4×4) reconstruction at even low C contents. For this case, models that do not necessarily involve C in the c(4×4) unit cells are more possible.

Acknowledgements

This work was supported by the EU RTN program SIGENET under grant HPRN-CT-1999-00123. C.G. acknowledges the hospitality of the Physics Department, University of Crete, and of

FORTH during a secondment from the Paul Scherrer Institute.

References

[1] T. Takaoka, T. Takagaki, Y. Igari, I. Kusunoki, Surf. Sci. 347 (1996) 105.
[2] K. Miki, K. Sakamoto, T. Sakamoto, Appl. Phys. Lett. 71 (1997) 3266.
[3] M.L. Shek, Surf. Sci 414 (1998) 353.
[4] R. Butz, H. Lüth, Surf. Sci. 411 (1998) 61.
[5] O. Leifeld, D. Grützmacher, B. Müller, K. Kern, E. Kaxiras, P.C. Kelires, Phys. Rev. Lett. 82 (1999) 972.
[6] H. Noremberg, G. Briggs, Surf. Sci. 430 (1999) 154.
[7] P. Sonnet, L. Stauffer, A. Selloni, A. De Vita, R. Car, L. Simon, M. Stoffel, L. Kubler, Phys. Rev. B 62 (2000) 6881.
[8] L. Simon, M. Stoffel, P. Sonnet, L. Kubler, L. Stauffer, A. Selloni, A. De Vita, R. Car, C. Pirri, G. Garreau, D. Aubel, J.L. Bischoff, Phys. Rev. B 64 (2001) 035306.
[9] I.N. Remediakis, E. Kaxiras, P.C. Kelires, Phys. Rev. Lett. 86 (2001) 4556.
[10] S.T. Jemander, H.M. Zhang, R.I.G. Uhrberg, G.V. Hansson, Phys. Rev. B 65 (2002) 115321.
[11] P.C. Kelires, E. Kaxiras, Phys. Rev. Lett. 78 (1997) 3479.
[12] H. Osten, M. Methfessel, G. Lippert, H. Rücker, Phys. Rev. B 52 (1995) 12179.
[13] H. Rücker, M. Methfessel, E. Bugiel, H.J. Osten, Phys. Rev. Lett. 72 (1994) 3578.
[14] P.C. Kelires, Surf. Sci. 418 (1998) L62.
[15] P.C. Kelires, J. Tersoff, Phys. Rev. Lett. 63 (1989) 1164.
[16] J. Tersoff, Phys. Rev. Lett. 74 (1995) 5080.
[17] M. Stoffel, L. Simon, D. Aubel, J.L. Bischoff, L. Kubler, Surf. Sci. 454–456 (2000) 201.
[18] G. Kresse, J. Hafner, Phys. Rev. B 47 (1993) 558.
[19] G. Kresse, J. Furthmüller, Comput. Mater. Sci. 6 (1996) 15.
[20] G. Kresse, J. Furthmüller, Phys. Rev. B 54 (1996) 11169.
[21] P. Hohenberg, W. Kohn, Phys. Rev. 136 (1964) B864.
[22] W. Kohn, L.J. Sham, Phys. Rev. 140 (1965) A1133.
[23] J.P. Perdew, Y. Wang, Phys. Rev. B 45 (1992) 13244.
[24] D. Vanderbilt, Phys. Rev. B 41 (1990) 7892.
[25] G. Kresse, J. Hafner, J. Phys.: Condens. Matter 6 (1994) 8245.
[26] P. Pulay, Chem. Phys. Lett. 73 (1980) 393.
[27] J. Tersoff, D.R. Hamann, Phys. Rev. B 31 (1985) 805.
[28] R.M. Tromp, R.J. Hamers, J.E. Demuth, Phys. Rev. Lett. 55 (1985) 1303.
[29] J. Tersoff, Phys. Rev. B 39 (1989) 5566.
[30] P.C. Kelires, Phys. Rev. Lett. 75 (1995) 1114.
[31] P.C. Kelires, Int. J. Mod. Phys. C 9 (1998) 357.
[32] N. Metropolis, A.W. Rosenbluth, M.N. Rosenbluth, A.H. Teller, E. Teller, J. Chem. Phys. 21 (1953) 1087.
[33] E. Kaxiras, Y. Bar-Yam, J. Joannopoulos, K. Pandey, Phys. Rev. Lett. 57 (1986) 106.
[34] E. Kaxiras, K. Pandey, Y. Bar-Yam, J. Joannopoulos, Phys. Rev. Lett. 56 (1986) 2819.
[35] J. Wang, T.A. Arias, J.D. Joannopoulos, Phys. Rev. B 47 (1993) 10497.
[36] N. Roberts, R. Needs, Surf. Sci. 236 (1990) 112.
[37] R.O. Jones, J. Chem. Phys. 110 (1999) 5189.
[38] P.C. Kelires, E. Kaxiras, J. Vac. Sci. Technol. B 16 (1998) 1687.
[39] O. Leifeld, A. Beyer, D. Grützmacher, K. Kern, Phys. Rev. B 66 (2002) 125312;
G. Hadjisavvas, Ph. Sonnet, P.C. Kelires, Phys. Rev. B 67 (2003) 241302(R).
[40] J.Y. Maeng, S. Kim, Surf. Sci. 482–485 (2001) 1445.